https://doi.org/10.5194/essd-2022-238
Preprint. Discussion started: 11 August 2022

Open Access Earth System Science Data Discussions

A new inventory of High Mountain Asia surge-type glaciers derived from multiple elevation datasets since the 1970s

Lei Guo[1], Jia Li[1], Amaury Dehecq[2], Zhiwei Li[1], Xin Li[3], Jianjun Zhu[1]

[1]School of Geo-science and Info-physics, Central South University, Changsha, 410083, China.
[2]Univ. Grenoble Alpes, IRD, CNRS, Grenoble INP, IGE, Grenoble, 38000, France.
[3]Institute of Tibetan Plateau Research, Chinese Academy of Sciences, Beijing, 100101, China.

Correspondence to: Jia Li (lijia20050710@csu.edu.cn)

Abstract. Surges are an important source of glacier hazards and complete surge-type glacier inventories are required for assessing glacier-related hazards. Glacier surge events in High Mountain Asia (HMA) are widely reported. However, the completeness of present inventories of HMA surge-type glaciers is constrained by the insufficient spatial and temporal coverage of glacier change observations, or by the limitations of the identification methods. In this paper, we established a new inventory of HMA surge-type glaciers based on the glacier surface elevation changes over four decades. Four kinds of elevation sources (KH-9 DEM, NASADEM, COP30 DEM, HMA8m DEM) were utilized to estimate the glacier surface elevation changes during two periods (1970s-2000 and 2000-2010s). In total 1015 surge-type glaciers were identified in HMA. Compared to the latest surge-type glacier inventory in HMA, our inventory incorporated 477 new surge-type glaciers. The number and area of surge-type glaciers accounted for ~2.49% (excluding glaciers less than 0.3 km^2) and ~23.32% of the total glacier number and glacier area in HMA, respectively. Considering that glacier outlines are usually composed of multiple tributaries within a glacier complex, the proportion of surge-related area may be overestimated, and the number of surge-type glaciers could be even larger. Surge-type glaciers were found in 21 of the 22 subregions of HMA (except for the Dzhungarsky Alatau), however, the density of surge-type glaciers is highly uneven. Surge-type glaciers are common in the northwest subregions (e.g., Pamir and Karakoram), but scarce in the peripheral subregions (e.g., Eastern Tien Shan, Eastern Himalaya, and Hengduan Shan). The inventory indicates that surge activity is more likely to occur for larger and longer glaciers. Besides, we found a potential relationship between the frequency of surge activities and regional glacier mass balance. The subregions with slightly negative or positive mass balance hold large clusters of surge-type glaciers, while those with severe glacier mass loss hold very few surge-type glaciers. In some subregions where glacier mass loss accelerated, the frequency of surge activities that occurred before 2000 was much higher than that after 2000. The inventory is available at: https://doi.org/10.5281/zenodo.6944979 (Guo et al., 2022).

Key words: High Mountain Asia, Surge-type glacier inventory, elevation change, KH-9, Digital Elevation Model (DEM)

1 Introduction

A surge is a glacier instability that translates into an abnormally fast flow over a period of a few months to years (Cogley et al., 2011). A surge-type glacier exhibits an active phase (surge) and a quiescent phase that may occur at quasi-periodic intervals (Jiskoot, 2011). Unlike the steady glacier flow that ice gradually moves downslope, the extreme active state of glacier surge is still an enigma. When a glacier surge occurs, a large volume of ice mass is transported downstream at a higher than average speed, and after the surge, the deposited ice melts fast. Glacier surge can induce several kinds of hazards, e.g., glacier lake outbursts (GLOF) when proglacial lakes exist (Round et al., 2017; Steiner et al., 2018), mudslides when the glacier is on a narrow-steep and moraine-based bed (Muhammad et al., 2021), or ice collapse when the glacier is already in a gravitational unsteady state (Kääb et al., 2018; Paul, 2019). Such mountain hazards have been frequently reported in recent decades (Shugar et al., 2021; An et al., 2021).

https://doi.org/10.5194/essd-2022-238
Preprint. Discussion started: 11 August 2022

Previous studies pointed out that the surge-type glaciers only occupy ~1% of total glaciers (Jiskoot, 2011; Sevestre and Benn, 2015). However, glacier surge is far more than an occasional behavior in some specific regions, such as the Alaska-Yukon (Clarke et al., 1986), Svalbard (Jiskoot et al., 2000; Farnsworth et al., 2016), and Karakoram-Pamir (Bhambri et al., 2017; Goerlich et al., 2020; Guillet et al., 2022). Accordingly, glacial hazards are frequent in these regions (Kääb et al., 2021). A complete inventory of surge-type glaciers inventory is a basis for the regional hazard assessment of glacier surges.

Generally, a surging glacier will exhibit four drastic changes: extreme speed-up (by a factor 10~1000 compared to normal conditions), distinct elevation change pattern, rapid terminus advance, and surface morphologic changes (medial or looped moraine, crevasses, etc.) (Jiskoot, 2011). Surge-type glaciers have been identified by many studies based on the observation of the above changes, e.g., glacier surface morphology (Clarke et al., 1986; Paul, 2015; Farnsworth et al., 2016), terminus position (Copland et al., 2011; Vale et al., 2021), or glacier motion (Quincey et al., 2011). The visual interpretation of glacier surface morphologic changes is easy to operate, but fraught with uncertainty due to the snow cover or the absence of supraglacial moraine (Jacquemart and Cicoira, 2022). To recognize abnormal changes in glacier motion, a long-term flow velocity time series is needed (Yasuda and Furuya, 2015; Round et al., 2017). Since the quiescent phase may last for decades and the image source for estimating the flow velocity is limited, the abnormal changes in glacier motion are prone to be missed. By combining observations of multiple features, the identification of surge-type glaciers could be more efficient and complete (Mukherjee et al., 2017; Goerlich et al., 2020; Guillet et al., 2022). However, the multi-factor method is hard to be implemented on a large spatial scale or a long temporal scale due to the deficiency of data acquisitions. By contrast, the recognition of abnormal surface elevation changes is an effective way to identify the surge-type glaciers (Vijay and Braun, 2018; Lv et al., 2019; Guillet et al., 2022), as its source datasets can satisfy the requirement of spatial-temporal coverage with comparatively fewer acquisitions.

Except for the polar regions, High Mountain Asia (HMA) is the most densely glacierized region in the world. Within the HMA range, several subregions are famous for the concentration of surge-type glaciers as well as the anomalous glacier mass balance (Hewitt, 2005; Gardelle et al., 2013; Farinotti et al., 2020). The inventories of surge-type glaciers have been established for some subregions like the Karakoram (Bhambri et al., 2017), West-Kunlun (Yasuda and Furuya, 2015), Pamir (Goerlich et al., 2020), Tien Shan (Mukherjee et al., 2017; Zhou et al., 2021). Sevestre and Benn (2015) presented the first global surge-type glacier inventory by reanalyzing historical reports from 1861 to 2013. However, it was compiled from various data sources (publications, reports, etc.) with inconsistent spatial-temporal coverage, which makes it difficult to ensure accuracy and completeness. Vale et al. (2021) identified 137 surge-type glaciers across HMA by detecting surge-induced terminus change and morphologic changes from Landsat images from 1987 to 2019. The number is obviously underestimated, because it is smaller than the numbers of previous subregional inventories (Bhambri et al., 2017; Goerlich et al., 2020). Guillet et al. (2022) presented a new surge-type glacier inventory of HMA by identifying multiple glacier change features. In total 666 surge-type glaciers were identified across HMA. However, the glacier change observation period is shorter than two decades (2000-2018), and therefore some surge-type glaciers with relatively long cycles may be missed.

In this paper, we aimed to build a more complete surge-type glacier inventory across HMA based on glacier surface elevation change observations over four decades. A workflow was developed to obtain the historical glacier surface elevation change from multiple datasets, including the KH-9 DEM (1970s), NASADEM (2000), COP30 DSM (2011-2014), and HMA8m DEM (2002-late 2016). Glaciers in the new inventory were divided into four classes of confidence in surge detection, based on the glacier elevation change pattern. Besides, the geometric characteristics of surge-type glaciers were thoroughly analyzed to clarify the factors affecting the glacier surge activity.

https://doi.org/10.5194/essd-2022-238
Preprint. Discussion started: 11 August 2022

2 Study region

High Mountain Asia consists of the Qinghai-Tibet Plateau and the surrounding regions, including the Karakoram, Pamir, Himalayas, and Tien Shan. According to the Randolph Glacier Inventory version 6.0, HMA hosts 95536 glaciers covering a total area of ~97605 km^2, equal to 13.8% of the global glacier area (Pfeffer et al., 2014; RGI Consortium, 2017). The Hindu Kush Himalayan Monitoring and Assessment Programme divided HMA into 22 subregions (Fig. 4) (Bolch et al., 2019). Different subregions are influenced by different air currents, such as the South Asia monsoon, the East Asia monsoons, and the westerlies (Bolch et al., 2012; Maussion et al., 2014). Glacier mass balance across HMA was found to be heterogeneous in the past decades (Gardelle et al., 2013; Brun et al., 2017; Shean et al., 2020). In particular, glaciers in the Pamir-Karakoram-West Kunlun region had a slightly positive or balanced mass budget (Hewitt, 2005; Zhou et al., 2017; Farinotti et al., 2020), while those in the Eastern Himalayas, Nyainqentanglha and Hengduan Shan mountain ranges experienced substantial ice loss (Maurer et al., 2019).

3 Datasets

3.1 Elevation Data

The NASADEM is mainly reprocessed from the C-band SRTM (Shuttle Radar Topography Mission) images. Among the current global DEMs, the NASADEM has the shortest source data acquisition period (~11/02/2000~22/02/2000) (Farr et al., 2007). Based on an improved production flow, the NASADEM has a better performance than the earlier SRTM void-free product in most regions (Crippen et al., 2016). The NASADEM was employed as the reference elevation source because its acquisition time, 2000, is suitable to divide the elevation change observations to before and after 21st century with moderate time span (one or two decades). Each tile of the product has an extent of 1°× 1° and a pixel spacing of 1 arc-second (see Fig. 1a). In total 313 tiles were downloaded from NASA LP DAAC (https://e4ftl01.cr.usgs.gov/MEASURES/NASADEM_HGT.001/).

Another global DEM we utilized is the newly released Copernicus DEM GLO-30-DGED (i.e., COP30 DEM). The COP30 DEM was edited from the delicate WorldDEM™, which was generated based on the TanDEM-X mission. The global RMSE of COP30 DEM is ±1.68 m (AIRBUS, 2020). Several studies have pointed out that this DEM is the most reliable open-access DEM to date (Purinton and Bookhagen, 2021; Guth and Geoffroy, 2021). The source images of COP30 DEM were mostly acquired between 2011 and 2014, and therefore COP30 DEM is suitable to represent the surface elevation in the 2010s. Like the NASADEM, the COP30 DEM has a pixel spacing of 1 arc second. Each tile of product has an extent of 1°× 1°. In total 313 tiles were downloaded through ESA Panda (https://panda.copernicus.eu/web/cds-catalogue/panda).

The High Mountain Asia 8-meter DEM (HMA8m DEM) was also utilized in this study. The HMA8m DEM was generated from high-resolution commercial optical satellite stereo images, including WorldView-1/2/3, GeoEye-1, and Quickbird-2 (Shean et al., 2020), through an automated photogrammetry workflow that is integrated with multiple error-control processes (Shean et al., 2016). This DEM was originally produced for the mass balance estimation of HMA glaciers, so it covered most of the glacierized regions in HMA. In total 3598 DEM tiles were downloaded from National Snow and Ice Data Center (https://nsidc.org/data/HMA_DEM8m_MOS/versions/1). About 95% of them were acquired between 2010 and 2016 (Fig. 1b). Due to the data voids and inconsistent acquisition time, the HMA8m DEM was taken as a supplementary elevation source to increase the observations in the 2010s.

The Hexagon KeyHole-9 (KH-9) imagery was acquired in the 1970s. It is one of the earliest near-global satellite stereo image source. The KH-9 imagery is characterized by a spatial resolution of 6-9 m, a wide coverage (130 km x 260 km), and a 70% forward overlap (Surazakov and Aizen, 2010). Many studies have utilized this imagery to estimate historical glacier surface elevation (Holzer et al., 2015; Zhou et al., 2017; Maurer et al., 2019). The KH-9 DEMs used in this study were generated

https://doi.org/10.5194/essd-2022-238
Preprint. Discussion started: 11 August 2022

through the automated ASPy pipeline (Dehecq et al., 2020). The methodology, validated in the European Alps and Alaska achieved a vertical accuracy of ~5m (68% confidence level). For more details on the method of KH-9 DEM generation, please refer to Dehecq et al. (2020). In total 238 DEMs with a resolution of 48 m were generated from the KH-9 images acquired between 1973 and 1980. The KH-9 DEMs were utilized to represent the glacier surface elevation in the 1970s (See Fig. 1c).

3.2 Glacier inventory

The Randolph Glacier Inventory V6.0 (RGI6.0) (RGI Consortium, 2017) outlines were utilized as templates for the surge-type glacier inventory. RGI6.0 provides the spatial extent and basic properties of each glacier with high-level quality control. The glacier information in the attributes table was used to interpret the geometric characteristics of surge-type glaciers.

4 Methodology

4.1 Estimation of glacier surface elevation change

The four kinds of DEMs have different coordinate references, vertical references, and data formats. Firstly, all DEMs were converted to float GeoTiff format. For datasets with quality files (NASADEM and the COP30 DEM), the DEM were preprocessed to mask out the pixels of low quality. The poor pixels of COP30 DEM tile were determined through the attached height error map (with values larger than 2.5 m) and water body map (with values not equal to zero). The NASADEM was directly masked with the attached water mask file. Subsequently, the coordinate system, map projection, and vertical reference of all DEMs tiles were unified as the WGS84 coordinate system, HMA Albers Equal Area projection (Shean et al., 2020), and WGS84 ellipsoid. The glacier surface elevation changes during 2000-2010s were derived by subtracting the NASADEM from the COP30 DEM and HMA8m DEM, and those during 1970s-2000 were derived by subtracting the KH-9 DEM from the NASADEM.

An automated DEM differencing workflow for large-scale glacier surface elevation change estimation was developed based on the *demcoreg* package presented by Shean et al. (2019). The workflow integrated multiple DEM co-registration approaches, the polynomial fit of tilt error, and other adaptive outlier removal approaches that was operated based on the observations over stable regions. Hence, a mask that excluded the water bodies and glacierized regions was generated in advance. Before differencing, the two DEMs need to be co-registered, because a small geolocation shift can result in considerable elevation change errors in high mountain regions. The efficient analytical DEM co-registration method presented by Nuth and Kääb (2011) was used to eliminate the relative geolocation shift between DEMs. This method assumes the geolocation shift vectors of all DEM pixels are identical. However, for the global DEM products like NASADEM and COP30 DEM, a DEM tile was usually mosaiced from multiple DEM patches, and the geolocation shift vectors at different parts of the DEM tile may be different. In view of this problem, we developed a block-wise version of the analytical DEM co-registration method to reduce the impacts of geolocation accuracy anisotropy of a DEM tile. Each DEM tile was divided into m×n blocks, and the DEM shifts were estimated for each block. Then, the m×n groups of shift parameters were merged into one group of shift parameters through a cubic interpolation. Technically, the estimated shift parameters become increasingly representative as the block size decreases. However, the fitting of shift parameters requires a certain number of samples. The final block size was set to 300×300 pixels to reach the best balance between the representativeness and estimation accuracy of shift parameters. Besides, we found that the block-wise co-registration method could result in wrong fitting of shift parameters over flat regions. To deal with this, a threshold of mean slope (10°) was set to classify the DEMs into the flat and the hilly categories, and the original global co-registration method (Nuth and Kääb, 2011) was applied to the flat ones.

Due to the residual orbital error of satellite images, the elevation difference maps often showed planimetric trends. This type of systematic error was fitted as a universal surface trend using a quadratic polynomial model based on the observations in stable regions, and then was removed from the elevation difference tile (Li et al., 2017). Besides, due to the jitter of the SAR

https://doi.org/10.5194/essd-2022-238
Preprint. Discussion started: 11 August 2022

antenna and optical mapping camera, the elevation difference maps often showed stripes (i.e., band-like artifacts) (Yamazaki et al., 2017). To eliminate the stripes, the elevation difference map was converted to the frequency domain through the Fast-Fourier-Transform method. Since the cyclic values have a high frequency in the power spectral density map, a threshold of frequency was set to separate the stripes components from the normal elevation differences. The de-stripping was completed after the backward transformation. Finally, the outliers of elevation difference maps were reduced through the 3-sigma threshold criteria.

Finally, three elevation change maps were calculated: the COP30 DEM – NASADEM, the HMA8m DEM – NASADEM, and the NASADEM – KH-9 DEM. The first two elevation change maps were used for the surge-type glacier identification during the period 2000-2010s, and the last one during the period 1970s-2000. In total, our elevation change observations covered ~92% of the total glacier area within HMA in 2000-2010s, and ~77% in 1970s-2000. Gaps in observations were mainly due to: 1) data voids and incomplete coverage of original DEMs tile, which was the main cause for the KH-9 DEMs and HMA8m DEM related results; 2) gross error removal during the elevation change calculations, which led to the scattered holes in the COP30 DEM related results.

4.3 Surgy-type glacier identification

In general, a typical glacier surge cycle can be divided into three phases (Jiskoot, 2011): 1) the build-up phase, characterized by remarkable thickening in the upper reaches; 2) the active phase, characterized by remarkable thinning in the upper reaches and thickening in the lower reaches; 3) the post-surge phase, characterized by strong down-wasting in the lower reaches. The classical method of identifying surge-type glaciers is to recognize the combination of marked upper thinning and lower thickening in the longitudinal direction. However, to distinguish the surge-type glaciers in the build-up or post-surge phase, careful comparison with surrounding glaciers is required. It is difficult to identify a surge-type glacier in the build-up or post-surge phase with a mathematical index. Moreover, multiple surge activities may occur at the tributaries of a large glacier system, especially in the Karakoram (Bhambri et al., 2022). In this study we established a four-class indicator to distinguish the surge possibility through the visual interpretation of glacier elevation change patterns:

I) ‘verified’: either of 1) a glacier having obviously thickened terminus (e.g. +30m); 2) a glacier having a combination of marked upper thinning (e.g. -20m) and lower thickening (e.g. +20m) in the longitudinal direction; 3) a glacier having a combination of marked upper thickening (e.g. +20m) and lower thinning (e.g. -30m) in the longitudinal direction.

II) ‘multiple’: a glacier having a ‘verified’ surge-type trunk and one or more ‘verified’ surge-type tributaries, or having two or more ‘verified’ surge-type tributaries.

III) ‘probable’: a glacier having a combination of moderate upper thinning (e.g. -15m) and lower thickening (e.g. +15m) in the longitudinal direction while its neighbours have no such signals.

IV) ‘possible’: either of 1) a glacier only having lower thinning that is much stronger (e.g. two times) than the normal melting of surrounding glaciers (typically lower than -1 m/year); 2) a glacier only having upper thickening that is much more evident (e.g. two times) than surrounding glaciers (typically lower than +0.5 m/year).

Note that, the specific values of elevation change mentioned above were for information only. Because of the diversity in the regional elevation change patterns under different climate or topographic conditions, the thresholds may vary spatially.

The identification of surge-type glaciers was conducted separately according to the three groups of elevation change observations. The sub-inventory based on the results of the NASADEM – KH-9 DEM was generated to represent the period of 1970s-2000.The two sub-inventories based on the COP30 DEM – NASADEM and the HMA8m DEM – NASADEM were generated individually and merged to represent the period of 2000-2010s. For the final inventory, the two sub-inventories were merged together. The merging of sub-inventories followed the principle of possibility. If a glacier was identified as a surge-type glacier in one of two periods, it was deemed as a surge-type glacier in the final inventory. If a glacier was identified as a surge-type glacier in both two periods but attached with different indicators, its indicator in the final inventory was taken from

https://doi.org/10.5194/essd-2022-238
Preprint. Discussion started: 11 August 2022

the indicator having a higher possibility. The possibility of four types of indicators follows the order: 'multiple' > 'verified' > 'probable' > 'possible'. For example, a glacier was identified as a multiple surge-type glacier in the period of 1970s-2000, and was identified as a probably surge-type glacier in the period of 2000-2010s, it was deemed as a 'multiple' surge-type glacier in the final inventory. To ensure the consistency of the result, the work of identifying surge-type glaciers was done by the same person. Figure 2 shows an example of surge-type glacier identification results.

5 Results

5.1 Surge-type glaciers identification

A total of 807 and 570 surge-type glaciers were identified during the periods of 2000-2010s and 1970s-2000, respectively. Due to the incomplete coverage and data voids of KH-9 DEMs, fewer surge-type glaciers were identified during the period of 1970s-2000. Finally, 1015 glaciers across the HMA were identified as surge-type glaciers (Fig. 3). The identified surge-type glaciers consisted of 70 'multiple' ones, 634 'verified' ones, 196 'probable' ones, and 115 'possible' ones. The area of 'multiple' and 'verified' surge-type glaciers accounted for ~40% and ~43% of the total surge-type glacier area (9112.97 km^2), respectively. When merging the identification results of the two periods, 36 probable and 12 possible surge-type glaciers identified during 2000-2010s turned to be 'verified' surge-type glaciers during 1970s-2000. Meanwhile, 45 'probable" and 22 'possible' surge-type glaciers identified during 1970s-2000 turned out to be 'verified' surge-type glaciers during 2000-2010s. Thanks to an almost complete coverage of the elevation change observations, we were able to classify all glaciers in HMA. Table 1 shows the detailed surge-type glacier identification results.

5.2 Distribution of surge-type glaciers

Surge-type glaciers were identified in 21 subregions of HMA (except for the Dzhungarsky Alatau), however, the density of identified surge-type glaciers is far from even (Fig. 3). The surge-type glaciers are common in the northwest regions, sporadic in the inner regions, and scarce in the peripheral regions. Figure 4 and Table 2 show the ratios of surge-type glacier number and area in each subregion. Considering the area of the smallest identified surge-type glacier is 0.37 km^2, we only took the glaciers larger than 0.30 km^2 in the glacier number related ratio. The number (1015) and area (22766.52 km^2) of identified surge-type glaciers accounted for ~2.49% and ~23.32% of the total glacier number and glacier area in HMA, respectively. Among the 22 subregions, the Karakoram is the largest cluster of surge-type glaciers. In total 374 surge-type glaciers were identified in the Karakoram, and 32 of them belonged to 'multiple' surge-type. The number of 'multiple' surge-type glaciers in the Karakoram accounted for 45.7% of HMA. Note that the 'multiple' surge-type glaciers are usually extra-large glaciers (say 100 km^2 or larger). Hence, the area of surge-type glaciers in the Karakoram (11324.78 km^2) is much larger than in other subregions. More than half of the glacier area in the Karakoram belongs to surge-type glaciers. The Pamirs, composed of the Eastern Pamir, Western Pamir and Pamir Alay, hosts 282 surge-type glaciers. About 33.8% of the glacier area in the Eastern and Western Pamir belong to surge-type glaciers. Surge-type glaciers are also common in the Western Kunlun. In total 96 surge-type glaciers were identified in the West Kunlun, and their area accounted for 34.7% of the glacier area. The Central Tien Shan has the fourth largest surge-type glacier area. In total 62 surge-type glaciers were identified in the Central Tien Shan, which accounted for 19.5% of the glacier area. The Karakoram, Pamirs, West Kunlun, and Central Tien Shan nourished ~80% of the surge-type glaciers across HMA. Figure 5 shows the distribution of identified surge-type glaciers in these four regions. Within interior HMA subregions (including the Tibetan Interior Mountains, Eastern Kunlun Shan, and Tanggula Shan), the number of surge-type glaciers only covered about 2% of the total glacier number, but the area accounted for about 20% of the total glacial area. Surge-type glaciers in these regions generally gathered in some watersheds. Similar localized surge-type glacier clusters were also found in the Nyainqentanglha, Northern and Western Tien Shan, and Central Himalaya, but the corresponding area ratios are much lower. We also found 'multiple' surge-type glaciers in the Western/Eastern Himalaya and Qilian Shan where surge events were rarely reported.

https://doi.org/10.5194/essd-2022-238
Preprint. Discussion started: 11 August 2022

5.3 Geometric characteristics of surge-type glaciers

We divided all glaciers larger than 0.30 km^2 into 11 classes according to their area, and calculated the ratios of surge-type glacier number and area in each class. Note that the smallest identified surge-type glacier is 0.37 km^2. As shown in Figure 6, surge-type glaciers were found in all classes. For the four classes in which glaciers are larger than 50 km^2, the ratios of surge-type glaciers area and number were about 72.4% and 62.9%, respectively. For the two classes in which glaciers are larger than 300 km^2, the ratios of surge-type glaciers area and number were over 85%. All the glaciers larger than 500 km^2 were identified as 'multiple' surge-type glaciers. Fig. 6 shows that both the ratios of surge-type glacier area and number became increasingly high as the glacier class size increased, which indicated that the larger glaciers are more likely to be surge-type glaciers.

We also analyzed the distribution of surge-type glacier number and area in different aspects. To minimize the discrepancy due to the large gap in the sample sizes (~40000 vs. 1015), we randomly sampled 1015 nonsurge-type glaciers 1000 times, and calculated the distribution of sampled nonsurge-type glaciers for each time. As shown in Fig. 7, both the number and area of glaciers facing the north are the largest, and then followed by those facing the northwest and northeast. In each aspect, the standard deviations (STD) of glacier numbers calculated from the 1000 repetitions of nonsurge-type glacier samples is less than 1.4%, and the STD of glacier area is less than 3.8%, which means the impact of the sample sizes on the glacier distribution is negligible. The number of surge-type glaciers facing the north accounted for ~33% of the total surge-type glacier number, and their area accounted for ~28% of all surge-type glacier area. In particular, the number and area ratios of surge-type glaciers facing the north are obviously higher than the non-surge-type glacier facing the north, while the number and area ratios of surge-type glaciers facing the northwest are obviously lower than the nonsurge-type glacier facing the northwest.

Figure 8 illustrates the comparisons between the basic geometric properties of surge-type and nonsurge-type glaciers. As seen in figures 8a, 8b, and 8c, relative to nonsurge-type glaciers, surge-type glaciers generally have a larger area, wider elevation range (i.e., the highest glacier surface elevation minus the lowest), and longer flowline. The area of most surge-type glaciers is within the band of 3~50 km^2, and the median value is 8.20 km^2, much larger than that of nonsurge-type glaciers (0.74 km^2). The surface elevation ranges of most surge-type glaciers are within the band of 1000~2500 m, and the median value is 1482 m, much higher than that of the nonsurge-type glacier (574 m). The discrepancy in the length between the two kinds of glaciers is even more evident. The median value of the length of surge-type glaciers is 6590 m, about 3.5 times longer than that of the nonsurge-type glacier (1493 m). In terms of mean surface slope and median elevation, the values of the surge-type glaciers are less spread out than the nonsurge-type glaciers. However, the median values of the two kinds of glaciers are very close (see Figures 8d and 8e).

The correlation between different glacier geometric properties was analyzed through the bivariate scatterplots (see Figure 9). Among the glacier area, glacier length, and glacier surface elevation range, any two of them have an apparent positive correlation. The glacier mean slope has a moderate correlation with the glacier area, glacier length, and glacier elevation range. By contrast, the glacier median elevation has little correlation with glacier area, glacier length, glacier elevation range, and glacier mean slope. The correlation of any two geometric properties makes little difference between surge-type and nonsurge-type glaciers.

6 Discussion

6.1 Uncertainty analysis

The reliability of surge-type glacier identification is directly related to the accuracy of glacier surface elevation change. Assuming the uncertainties in surface elevation change are similar over glacierized areas and stable areas, we evaluated the glacier elevation change uncertainties based on elevation change observations in stable areas, whose true values are zeros. The normalized median absolute deviation (NMAD) is less sensitive to outliers and can be deemed as an alternative to standard deviation (Höhle and Höhle, 2009). Hence, the NMAD was used to denote the uncertainty of individual glacier surface

https://doi.org/10.5194/essd-2022-238
Preprint. Discussion started: 11 August 2022

elevation change tile (Li et al., 2017). Figure 10 shows the NMAD of elevation change observations in stable areas within each DEM differencing tile, which were used for the co-registration and biases removal during the glacier elevation change estimation. Due to large distortions in the KH-9 images, the NASADEM - KH-9 DEM results had the highest uncertainties. Benefiting from the advantages of bistatic SAR image pairs, the COP30 DEM has high quality, and the COP30 DEM related results had the lowest uncertainties. The HMA8m DEM related results had moderate uncertainties. The average NMAD of all DEM differencing tiles was smaller than 5 m. The significant elevation errors usually occurred in the highly rugged regions such as crests and horns. The terrain of glacier surface is relatively gentle, and therefore the uncertainties of glacier surface elevation changes should be lower than the estimated values. In general, the uncertainties of our elevation change results are well-controlled. Compared with the typical surface elevation change resulted from a glacier surge (tens to hundreds of meters), the magnitudes of uncertainties are very small. Similar to previous studies (Sevestre and Benn, 2015; Goerlich et al., 2020), the surge-type glacier identification in this study was completed through a manual qualitative interpretation way. It's difficult to provide a quantitative index to represent the uncertainty of surge identification. However, the four-class indicator of surge likelihood could aid that in a degree.

6.2 Characteristics of surge-type glaciers

The comparison between geometric characteristics of surge-type and nonsurge-type glaciers manifests that surge activity is more likely to occur in the glacier with a larger area, wider elevation range, and longer length (Fig. 8). Previous studies also reported this phenomenon (Barrand and Murray, 2006; Jiskoot, 2011; Sevestre and Benn, 2015; Mukherjee et al., 2017; Guillet et al., 2022). Larger area, wider elevation range, and longer length mean a larger glacier scale and more mass storage. Surge is a self-balancing process of a glacier to regulate its internal instability of thermal or hydrologic conditions which needs enough mass storage. For glaciers larger than 50 km^2, surge becomes common behavior, rather than accidental behavior (see Fig.6).

Fig. 8d shows that, in terms of mean surface slope, the values of the surge-type glaciers are more concentrated than the nonsurge-type glaciers, but the median values of the two kinds of glaciers are very close (see Figures 8d and 8e). Surge-type glaciers are larger and tend to have a mean slope that is less spread than smaller glaciers (Figure 9, 3rd row, 1st column), which is the reason why we observed a smaller spread for surge type glaciers on Figure 8d. As shown in Fig. 9, among the nonsurge-type glaciers, the small ones occupy a high proportion and their mean slope presents strong randomness. Previous studies have demonstrated that the surge-type glacier tend to have shallower slope (Jiskoot et al., 2000; Guillet et al., 2022), which is a consequence of the inverse relationship between the glacier slope and length (Clarke, 1991; Sevestre and Benn, 2015). However, the rule that smaller glaciers have a higher mean slope does not apply to very small glaciers. If we set a threshold of glacier area (say 1 km^2) when drawing Fig. 8d, the result could be different. As for the glacier median elevation, since it is almost irrelevant to the glacier area, glacier length, glacier elevation range, and glacier mean slope (see Fig. 9), it can be deemed as an irregular glacier index.

Besides, our results manifested that the ratio distribution of surge-type glaciers in eight aspects are slightly different from that of nonsugre-type glaciers (see Fig. 7). This is in line with the findings in previous studies (Bhambri et al., 2017; Goerlich et al., 2020). In particular, the ratio of surge-type glaciers is relatively higher than the non-surge type glaciers in the north direction, but lower in the northwest direction. This is mainly caused by the orientation of the mountains in Karakoram and Pamir. It is generally known that glaciers facing the north are more developed in HMA. Due to the orientation of the mountains, most of the large glaciers in Karakoram and Pamir flow toward the north and northeast. The number of large glaciers flowing towards the northwest is much less. Accordingly, the surge-type glaciers facing the north and northeast are much more than that facing the northwest (see Fig. 5). The number of surge-type glaciers in Karakoram and Pamir accounts for a considerable proportion of the total number of surge-type glaciers in HMA, and therefore the orientation of surge-type glaciers there has a great impact on the orientation distribution of surge-type glaciers in HMA.

https://doi.org/10.5194/essd-2022-238
Preprint. Discussion started: 11 August 2022

In the present inventory and analyses, we have not considered the impact of individual tributary surges. Multiple studies have demonstrated that the tributary surge is an usual behavior within HMA (Hewitt, 2007; Bhambri et al., 2022). Hence, when surges only occur in the tributaries within a glacier complex, biases could exist in the area related analyses. The surge-related area could be overestimated. Statistically speaking, a large mountain glacier is more likely to be classified as surge-type, due to the well-developed tributaries. This could also help with the interpretation that larger glaciers are more likely to surge (Fig. 6), and surge-type glaciers are more concentrated in the north direction (Fig. 7). Meanwhile, the frequent tributary surges may also lead to the underestimation of surge-type glacier number, because surges occur in more than one tributary in a glacier complex (correspond to the "multiple" surge-type class). However, the surging tributary is hard to separate from the glacier complex. As the surging mass of a tributary injecting into the trunk, the surge-related area could expand beyond the extent of the tributary, or occasionally, another surge in the glacier trunk could be activated (Guo et al., 2020).

The spatial distribution of surge-type glaciers in HMA presents strong heterogeneity. About 80% of identified surge-type glaciers were located in the northwest region including the Central Tien Shan, Pamirs, Karakoram, and West Kunlun, and their area occupied about 86% of the total identified surge-type glacier area (see Fig. 4 and Table 2). As discussed above, larger glaciers are more likely to be surge-type. The northwest regions generally hold more large glaciers, and therefore hold more surge-type glaciers. In other subregions, large glaciers are usually concentrated in some great ice fields, such as the Geladandong, Puruogangri, and Xinqingfeng. Accordingly, surge-type glaciers in these subregions are usually clustered in several watersheds.

Several studies have pointed out that glacier surge activities have little impact on the glacier mass balance (Gardelle et al., 2013; Bolch et al., 2017; Guillet et al., 2022). However, glacier mass balance may also affect the occurrence of glacier surge. Copland et al. (2011) concluded that the increase of glacier surges in the Karakoram could be related to the positive mass budget. The accumulated ice mass would accelerate a glacier to surge (Eisen et al., 2005; Kochtitzky et al., 2020), and the significant mass loss could prevent or postpone the surge in return (Dowdeswell et al., 1995). On a regional large scale, the relationship between mass balance and surge occurrence needs to be further analyzed. Our glacier elevation change maps of the period 2000-2010s are similar to that derived by Brun et al. (2017) and Shean et al. (2020). We found that, at the regional scale, the occurrence of surge-type glaciers is correlated with the regional glacier mass balance. The three subregions holding the largest clusters of surge-type glaciers, i.e., the Pamirs, Karakoram, and West Kunlun, are characterized by slightly negative or positive mass budgets, which is known as the 'Pamir-Karakoram-West Kunlun' anomaly (Brun et al., 2017). Likewise, the subregions Central Tien Shan, Tibetan Interior Mountains, and East Kunlun Shan, which hold the moderate clusters of surge-type glaciers, have glacier mass loss rates much lower than the average rates of HMA. By contrast, subregions with severe glacier mass loss hold the lowest surge-type glacier ratio, such as the Dzhungarsky Alatau, Hengduan Shan, and Eastern Himalaya.

Furthermore, we found that, in some subregions where glacier mass loss accelerated, the frequency of surge activities that occurred before 2000 is much higher than that after 2000. For example, only 2 out of the 29 surge-type glaciers identified in the Central Himalaya surged after 2000. In the Nyainqentanglha, all 16 surge-type glaciers were identified during the 1975s-2000 period. Maurer et al. (2019) reported that glacier mass loss accelerated in the Central Himalaya during the past 40 years, and Bhattacharya et al. (2021) reported that glacier mass loss accelerated in the Nyainqentanglha since 1960s. This could indicate a positive relationship between the glacier surge frequency and glacier mass budget on the regional scale of HMA. A glacier surge occurs when the gravitational potential energy exceeds a threshold, or the bottom water pressure exceeds a threshold. Technically, glaciers undergoing severe mass loss have difficulties to accumulate enough mass to initiate the surge activities. Also, the drainage system could be well-established with the excessive and continuous meltwater input at the glacier surface (Hubbard, 2011). This paper is focused on the surge-type glacier inventory in HMA. Further research is needed to corroborate whether the observed and projected glacier mass loss will reduce the incidence of glacier surges in the future.

https://doi.org/10.5194/essd-2022-238
Preprint. Discussion started: 11 August 2022

6.3 Comparison with previous surge-type glacier inventories

Guillet et al. (2022) presented a comprehensive surge-type glacier inventory of HMA for the period 2000-2018 from a multi-factor remote sensing approach. Thanks to a longer observation period, we have identified more surge-type glaciers than Guillet et al. (2022) in every subregion, especially in the Karakoram (374 vs. 223) and the Pamirs (282 vs. 223). Within our inventory, 538 surge-type glaciers were also identified by Guillet et al. (2022), i.e., 476 surge-type glaciers were newly identified in our study. Guillet et al. (2022) identified 666 surge-type glaciers, and the area of surge-type glacier occupies 19.5% of the total glacier area. We identified 1015 surge-type glaciers, and their area occupies 23.32% of the total glacier area. Hence, most of the newly identified glaciers are small glaciers. If considering only the period 2000-2010s for comparison, our inventory also documents more surge-type glaciers (807) than Guillet et al. (2022). Our results share 494 surge-type glaciers with Guillet et al.). For the period of 1970s-2000, we have identified 231 surge-type glaciers that were not included by Guillet's inventory. We owed the newly findings to the much longer observation period and the multi-level identification of the surge possibility (Guillet et al. (2022) only considered the "verified" type). However, 128 surge-type glaciers identified by Guillet et al. (2022) were missed in this study, and 52 'probable' and 19 'possible' surge-type glaciers in our new inventory were identified as 'verified' surge-type glaciers by Guillet et al. (2022). We attribute this to the deficiency of using a single criterion, because over the long observation period the elevation change signals caused by small-scale glacier surge activities may be diluted by the regular elevation changes. Besides, the DEMs used in this study were suffering from the data voids and incomplete spatial coverage, especially for the KH-9 DEM. The earlier termination of our observation period (2014-2016 vs. 2018) could also partly explain the discrepancies.

Multiple studies have identified surge-type glaciers in the Karakoram based on different data sources. For example, Bhambri et al. (2017) identified 221 surge-type glaciers (the tributaries of a glacier system are counted as individual glaciers) based on the glacier morphology changes detected from space-borne optical images acquired from 1972 to 2016, in-situ observations, and archive photos since the 1840s. Also, the boundary used by Bhambri et al. to define the extent of Karakoram is much smaller than that used in our inventory. A much smaller group of surge-type glaciers (88) were identified by Copland et al. (2011) based on a similar method and the data acquired between 1960 and 2013. Rankl et al. (2014) identified 101 surge-type glaciers in the Karakoram by detecting the changes in glacier surface velocity and terminus position between 1976 and 2012. The results of Guillet et al. (2022) should be more reliable than previous ones, because more criteria were used for identifying surge-type glaciers. Among the 223 surge-type glaciers in the Karakoram identified by Guillet et al. (2022), 182 and 10 ones were identified by us during the periods of 2000-2010s and 1970s-2000, respectively. The high coincidence between the two inventories indicates our surge-type glacier identification result is reliable.

In the Pamirs, Sevestre and Been (2015) identified 820 surge-type glaciers based on publications and reports, but Goerlich et al. (2020) reported only 206 surge activities based on the observations of glacier flow velocity, elevation change, etc. The number of surge activities identified by Goerlich et al. (2020) is in good agreement with that of Guillet et al. (2022). Taking the RGI6.0 glacier inventory as a reference, we found the identified 206 surges actually occurred in 176 RGI glacier complexes. Among the 176 surge-type glaciers identified by Goerlich et al. (2020), 156 were included in our inventory, and therefore 126 surge-type glaciers in the Pamir were newly identified in this study. The main cause for the result discrepancy is that the glacier elevation change observation conducted by Goerlich et al. (2020) only covered parts of the Western Pamir and only the observations before 2000 were used. The comparison demonstrated that 175 surge-type glaciers were identified by both this study (during 2000-2010s) and Guillet et al. (2022), which also manifests a high coincidence of the two results.

In the West Kunlun, Yasuda and Furuya (2015) reported 9 surge-type glaciers in the main range only, based on changes in glacier flow velocity and terminus position of 31 glaciers, and other 9 surge-type glaciers were found in the northwest part of the West Kunlun Shan by Chudley et al. (2019). A much larger number (60) were found by Guillet et al. (2022). However, our inventory has included 96 surge-type glaciers in the West Kunlun Shan, and 20 of them were identified during the period 1970s-2000. In Central Tien Shan, Mukherjee et al. (2017) identified 39 surge-type glaciers through the analysis of changes

https://doi.org/10.5194/essd-2022-238
Preprint. Discussion started: 11 August 2022

in surface elevation and morphology from 1964 to 2014, whereas 62 were identified in our studies. The insufficient coverage of elevation change observation (only covered the west part of the Central Tien Shan) may be the main reason for the discrepancy in identification results. Guillet et al. (2022) identified 54 surge-type glaciers during 2000-2018, in which 37 were confirmed in our inventory.

7 Conclusions

This study presented a new inventory of surge-type glaciers across the entire HMA range, which was accomplished based on the glacier surface elevation changes derived from multiple elevation sources. In total 1015 surge-type glaciers were identified in the new inventory. Through the analysis of geometric parameters, we found that surge-type glaciers generally have a greater area, length, and elevation range than nonsurge-type glaciers. Furthermore, combing the region-wide glacier mass balance measurements, we found that the frequency of surge occurrence decreased in several subregions that saw an accelerated mass loss. Benefiting from the long period and wide coverage of surface elevation change observations, our study identified much more surge-type glaciers in HMA than in previous studies. However, our inventory does not provide the surge duration period and the maximum flow velocity to describe the dynamic process of each glacier surge activity. Improvements should be made by combining multi-criteria identification methods. Considering the fact that surge-type glaciers are more widespread than we thought, the inventory presented in this study still needs further replenishment.

8 Data and code availability

The presented inventory is freely available at: https://doi.org/10.5281/zenodo.6944979 (Guo et al., 2022). The dataset is composed of two files including the inventory itself and the associated metadate file. The inventory is distributed in the format of GeoPackage vector file (.gpkg). The glacier polygons, geometric attributes of the inventory are compiled from the RGI v6.0. In total three fields are integrated in the attributes table to describe the surge likelihood of corresponding glacier with the four-class indicators mentioned in section 4.3. The description of each field in the attribute table is listed in Table 3. The metadata file is distributed in the format of QGIS metadata file (.qmd), which contains the description and details of the spatial/temporal information of the inventory.

The code used for elevation change estimation can be available at: https://github.com/TristanBlus/dem_coreg. This code was developed based on the *demcoreg* package (Shean et al., 2019).

Author contribution

J.L. and L.G. conceived this study and wrote the paper. L.G. developed the processing flow, complied the inventory and drew the figures with the support from J.L. A.D. generated the KH-9 DEM. A.D., Z.L. and X.L. helped with the results analysis and discussions and manuscript editing. Z.L., J.L. and J.Z. provided the funding acquisition. All authors have contributed and agreed to the published version of the manuscript.

Competing interest

The authors declare that they have no conflict of interest.

https://doi.org/10.5194/essd-2022-238
Preprint. Discussion started: 11 August 2022

Acknowledgments

The authors express gratitude to all institution that provide us the opensource dataset used in this study: the NASADEM from LP DAAC (https://e4ftl01.cr.usgs.gov/MEASURES/NASADEM_HGT.001/), the Copernicus DEM from Eruopean Space Agency (ESA) (https://spacedata.copernicus.eu/web/cscda/cop-dem-faq)., the HMA8m DEM processed by David Shean from National Snow and Ice Data Center (NSIDC) (https://nsidc.org/data/HMA_DEM8m_MOS/versions/1), and the Randolph Glacier Inventory Version 6.0 (http://www.glims.org/RGI/randolph.html).

Financial support

This work was supported by the Strategic Priority Research Program of Chinese Academy of Sciences (XDA20100101), the National Natural Science Foundation of China (41904006), the National Natural Science Fund for Distinguished Young Scholars (41925016), the Hunan Key Laboratory of remote sensing of ecological environment in Dongting Lake Area (No. 2021-010), the Fundamental Research Funds for the Central Universities of Central South University (2021zzts0265).

References

AIRBUS: Copernicus Digital Elevation Model Validation Report, AIRBUS Defence and Space GmbH, 2020.

An, B., Wang, W., Yang, W., Wu, G., Guo, Y., Zhu, H., Gao, Y., Bai, L., Zhang, F., Zeng, C., Wang, L., Zhou, J., Li, X., Li, J., Zhao, Z., Chen, Y., Liu, J., Li, J., Wang, Z., Chen, W., and Yao, T.: Process, mechanisms, and early warning of glacier collapse-induced river blocking disasters in the Yarlung Tsangpo Grand Canyon, southeastern Tibetan Plateau, Sci. Total Environ., 151652, doi:10.1016/j.scitotenv.2021.151652, 2021.

Barrand, N. E. and Murray, T.: Multivariate Controls on the Incidence of Glacier Surging in the Karakoram Himalaya, Arct. Antarct. Alp. Res., 38, 489–498, doi:10.1657/1523-0430(2006)38[489:MCOTIO]2.0.CO;2, 2006.

Bhambri, R., Hewitt, K., Kawishwar, P., and Pratap, B.: Surge-type and surge-modified glaciers in the Karakoram, Sci. Rep., 7, doi:10.1038/s41598-017-15473-8, 2017.

Bhambri, R., Hewitt, K., Haritashya, U. K., Chand, P., Kumar, A., Verma, A., Tiwari, S. K., and Rai, S. K.: Characteristics of surge-type tributary glaciers, Karakoram, Geomorphology, 403, 108161, doi:10.1016/j.geomorph.2022.108161, 2022.

Bolch, T., Kulkarni, A., Kaab, A., Huggel, C., Paul, F., Cogley, J. G., Frey, H., Kargel, J. S., Fujita, K., Scheel, M., Bajracharya, S., and Stoffel, M.: The State and Fate of Himalayan Glaciers, Science, 336, 310–314, doi:10.1126/science.1215828, 2012.

Bolch, T., Pieczonka, T., Mukherjee, K., and Shea, J.: Brief communication: Glaciers in the Hunza catchment (Karakoram) have been nearly in balance since the 1970s, The Cryosphere, 11, 531–539, doi:10.5194/tc-11-531-2017, 2017.

Bolch, T., Shea, J. M., Liu, S., Azam, F. M., Gao, Y., Gruber, S., Immerzeel, W. W., Kulkarni, A., Li, H., Tahir, A. A., Zhang, G., and Zhang, Y.: Status and Change of the Cryosphere in the Extended Hindu Kush Himalaya Region, in: The Hindu Kush Himalaya Assessment, edited by: Wester, P., Mishra, A., Mukherji, A., and Shrestha, A. B., Springer International Publishing, Cham, 209–255, doi:10.1007/978-3-319-92288-1_7, 2019.

Brun, F., Berthier, E., Wagnon, P., Kääb, A., and Treichler, D.: A spatially resolved estimate of High Mountain Asia glacier mass balances from 2000 to 2016, Nat. Geosci., 10, 668–673, doi:10.1038/ngeo2999, 2017.

Chudley, T. R. and Willis, I. C.: Glacier surges in the north-west West Kunlun Shan inferred from 1972 to 2017 Landsat imagery, J. Glaciol., 65, 1–12, doi:10.1017/jog.2018.94, 2019.

Clarke, G. K. C.: Length, width and slope influences on glacier surging, J. Glaciol., 37, 236–246, doi:10.3189/S0022143000007255, 1991.

Clarke, G. K. C., Schmok, J. P., Ommanney, C. S. L., and Collins, S. G.: Characteristics of surge-type glaciers, J. Geophys. Res. Solid Earth, 91, 7165–7180, doi:10.1029/JB091iB07p07165, 1986.

https://doi.org/10.5194/essd-2022-238
Preprint. Discussion started: 11 August 2022

481 Cogley, J. G., Arendt, A. A., Bauder, A., Braithwaite, R. J., Hock, R., J, B., R., Jansson, P., Kaser, G., Moller, M., Nicholson,
482 L., Rasmussen, L. A., and Zemp, M.: Glossary of glacier mass balance and related terms, IACS Contribution No.2, UNESCO,
483 Paris, 2011.
484 Copland, L., Sylvestre, T., Bishop, M. P., Shroder, J. F., Seong, Y. B., Owen, L. A., Bush, A., and Kamp, U.: Expanded and
485 Recently Increased Glacier Surging in the Karakoram, Arct. Antarct. Alp. Res., 43, 503–516, 2011.
486 Crippen, R., Buckley, S., Agram, P., Belz, E., Gurrola, E., Hensley, S., Kobrick, M., Lavalle, M., Martin, J., Neumann, M.,
487 Nguyen, Q., Rosen, P., Shimada, J., Simard, M., and Tung, W.: NASADEM global elevation model: methods and progress,
488 ISPRS - Int. Arch. Photogramm. Remote Sens. Spat. Inf. Sci., XLI-B4, 125–128, doi:10.5194/isprsarchives-XLI-B4-125-2016,
489 2016.
490 Dehecq, A., Gardner, A. S., Alexandrov, O., McMichael, S., Hugonnet, R., Shean, D., and Marty, M.: Automated Processing
491 of Declassified KH-9 Hexagon Satellite Images for Global Elevation Change Analysis Since the 1970s, Front. Earth Sci., 8,
492 566802, doi:10.3389/feart.2020.566802, 2020.
493 Dowdeswell, J. A., Hodgkins, R., Nuttall, A.-M., Hagen, J. O., and Hamilton, G. S.: Mass balance change as a control on the
494 frequency and occurrence of glacier surges in Svalbard, Norwegian High Arctic, Geophys. Res. Lett., 22, 2909–2912,
495 doi:10.1029/95GL02821, 1995.
496 Eisen, O., Harrison, W. D., Raymond, C. F., Echelmeyer, K. A., Bender, G. A., and Gorda, J. L. D.: Variegated Glacier, Alaska,
497 USA: a century of surges, J. Glaciol., 51, 399–406, doi:10.3189/172756505781829250, 2005.
498 Farinotti, D., Immerzeel, W. W., Kok, R., Quincey, D. J., and Dehecq, A.: Manifestations and mechanisms of the Karakoram
499 glacier Anomaly, Nat. Geosci., 13, 8–16, doi:10.1038/s41561-019-0513-5, 2020.
500 Farnsworth, W. R., Ingólfsson, Ó., Retelle, M., and Schomacker, A.: Over 400 previously undocumented Svalbard surge-type
501 glaciers identified, Geomorphology, 264, 52–60, doi:10.1016/j.geomorph.2016.03.025, 2016.
502 Farr, T. G., Rosen, P. A., Caro, E., Crippen, R., Duren, R., Hensley, S., Kobrick, M., Paller, M., Rodriguez, E., Roth, L., Seal,
503 D., Shaffer, S., Shimada, J., Umland, J., Werner, M., Oskin, M., Burbank, D., and Alsdorf, D.: The Shuttle Radar Topography
504 Mission, Rev. Geophys., 45, RG2004, doi:10.1029/2005RG000183, 2007.
505 Gardelle, J., Berthier, E., Arnaud, Y., and Kääb, A.: Region-wide glacier mass balances over the Pamir-Karakoram-Himalaya
506 during 1999–2011, Cryosphere Discuss., 7, 975–1028, doi:10.5194/tcd-7-975-2013, 2013.
507 Goerlich, F., Bolch, T., and Paul, F.: More dynamic than expected: an updated survey of surging glaciers in the Pamir, Earth
508 Syst. Sci. Data, 12, 3161–3176, doi:10.5194/essd-12-3161-2020, 2020.
509 Guillet, G., King, O., Lv, M., Ghuffar, S., Benn, D., Quincey, D., and Bolch, T.: A regionally resolved inventory of High
510 Mountain Asia surge-type glaciers, derived from a multi-factor remote sensing approach, The Cryosphere, 16, 603–623,
511 doi:10.5194/tc-16-603-2022, 2022.
512 Guo, L., Li, J., Li, Z., Wu, L., Li, X., Hu, J., Li, H., Li, H., Miao, Z., and Li, Z.: The Surge of the Hispar Glacier, Central
513 Karakoram: SAR 3-D Flow Velocity Time Series and Thickness Changes, J. Geophys. Res. Solid Earth, 125,
514 doi:10.1029/2019JB018945, 2020.
515 Guth, P. L. and Geoffroy, T. M.: LiDAR point cloud and ICESat-2 evaluation of 1 second global digital elevation models:
516 Copernicus wins, Trans. GIS, 25, 2245–2261, doi:10.1111/tgis.12825, 2021.
517 Hewitt, K.: The Karakoram Anomaly? Glacier Expansion and the 'Elevation Effect,' Karakoram Himalaya, Mt. Res. Dev., 25,
518 332–340, doi:10.1659/0276-4741(2005)025[0332:TKAGEA]2.0.CO;2, 2005.
519 Hewitt, K.: Tributary glacier surges: an exceptional concentration at Panmah Glacier, Karakoram Himalaya, J. Glaciol., 53,
520 181–188, doi:10.3189/172756507782202829, 2007.
521 Höhle, J. and Höhle, M.: Accuracy assessment of digital elevation models by means of robust statistical methods, ISPRS J.
522 Photogramm. Remote Sens., 64, 398–406, doi:10.1016/j.isprsjprs.2009.02.003, 2009.

https://doi.org/10.5194/essd-2022-238
Preprint. Discussion started: 11 August 2022

523 Holzer, N., Vijay, S., Yao, T., Xu, B., Buchroithner, M., and Bolch, T.: Four decades of glacier variations at Muztagh Ata
524 (eastern Pamir): a multi-sensor study including Hexagon KH-9 and Pléiades data, The Cryosphere, 9, 2071–2088,
525 doi:10.5194/tc-9-2071-2015, 2015.
526 Hubbard, B.: Subglacial Drainage System, in: Encyclopedia of Snow, Ice and Glaciers, edited by: Singh, V. P., Singh, P., and
527 Haritashya, U. K., Springer Netherlands, Dordrecht, 1095–1099, doi:10.1007/978-90-481-2642-2_545, 2011.
528 Jacquemart, M. and Cicoira, A.: Hazardous Glacier Instabilities: Ice Avalanches, Sudden Large-Volume Detachments of Low-
529 Angle Mountain Glaciers, and Glacier Surges, in: Treatise on Geomorphology, Elsevier, 330–345, doi:10.1016/B978-0-12-
530 818234-5.00188-7, 2022.
531 Jiskoot, H.: Glacier Surging, in: Encyclopedia of Snow, Ice and Glaciers, edited by: Singh, V. P., Singh, P., and Haritashya,
532 U. K., Springer Netherlands, Dordrecht, 415–428, doi:10.1007/978-90-481-2642-2_559, 2011.
533 Jiskoot, H., Murray, T., and Boyle, P.: Controls on the distribution of surge-type glaciers in Svalbard, J. Glaciol., 46, 412–422,
534 doi:10.3189/172756500781833115, 2000.
535 Kääb, A., Leinss, S., Gilbert, A., Bühler, Y., Gascoin, S., Evans, S. G., Bartelt, P., Berthier, E., Brun, F., Chao, W.-A., Farinotti,
536 D., Gimbert, F., Guo, W., Huggel, C., Kargel, J. S., Leonard, G. J., Tian, L., Treichler, D., and Yao, T.: Massive collapse of
537 two glaciers in western Tibet in 2016 after surge-like instability, Nat. Geosci., 11, 114–120, doi:10.1038/s41561-017-0039-7,
538 2018.
539 Kääb, A., Jacquemart, M., Gilbert, A., Leinss, S., Girod, L., Huggel, C., Falaschi, D., Ugalde, F., Petrakov, D., Chernomorets,
540 S., Dokukin, M., Paul, F., Gascoin, S., Berthier, E., and Kargel, J. S.: Sudden large-volume detachments of low-angle mountain
541 glaciers – more frequent than thought?, The Cryosphere, 15, 1751–1785, doi:10.5194/tc-15-1751-2021, 2021.
542 Kochtitzky, W., Winski, D., McConnell, E., Kreutz, K., Campbell, S., Enderlin, E. M., Copland, L., Williamson, S., Main, B.,
543 and Jiskoot, H.: Climate and surging of Donjek Glacier, Yukon, Canada, Arct. Antarct. Alp. Res., 52, 264–280,
544 doi:10.1080/15230430.2020.1744397, 2020.
545 Li, J., Li, Z., Zhu, J., Li, X., Xu, B., Wang, Q., Huang, C., and Hu, J.: Early 21st century glacier thickness changes in the
546 Central Tien Shan, Remote Sens. Environ., 192, 12–29, doi:10.1016/j.rse.2017.02.003, 2017.
547 Lv, M., Guo, H., Lu, X., Liu, G., Yan, S., Ruan, Z., Ding, Y., and Quincey, D. J.: Characterizing the behaviour of surge- and
548 non-surge-type glaciers in the Kingata Mountains, eastern Pamir, from 1999 to 2016, The Cryosphere, 13, 219–236,
549 doi:10.5194/tc-13-219-2019, 2019.
550 Maurer, J. M., Schaefer, J. M., Rupper, S., and Corley, A.: Acceleration of ice loss across the Himalayas over the past 40 years,
551 Sci. Adv., 5, eaav7266, doi:10.1126/sciadv.aav7266, 2019.
552 Maussion, F., Scherer, D., Mölg, T., Collier, E., Curio, J., and Finkelnburg, R.: Precipitation Seasonality and Variability over
553 the Tibetan Plateau as Resolved by the High Asia Reanalysis, J. Clim., 27, 1910–1927, doi:10.1175/JCLI-D-13-00282.1, 2014.
554 Muhammad, S., Li, J., Steiner, J. F., Shrestha, F., Shah, G. M., Berthier, E., Guo, L., Wu, L., and Tian, L.: A holistic view of
555 Shisper Glacier surge and outburst floods: from physical processes to downstream impacts, Geomat. Nat. Hazards Risk, 12,
556 2755–2775, doi:10.1080/19475705.2021.1975833, 2021.
557 Mukherjee, K., Bolch, T., Goerlich, F., Kutuzov, S., Osmonov, A., Pieczonka, T., and Shesterova, I.: Surge-Type Glaciers in
558 the Tien Shan (Central Asia), Arct. Antarct. Alp. Res., 49, 147–171, doi:10.1657/AAAR0016-021, 2017.
559 Nuth, C. and Kääb, A.: Co-registration and bias corrections of satellite elevation data sets for quantifying glacier thickness
560 change, The Cryosphere, 5, 271–290, doi:10.5194/tc-5-271-2011, 2011.
561 Paul, F.: Revealing glacier flow and surge dynamics from animated satellite image sequences: examples from the Karakoram,
562 The Cryosphere, 9, 2201–2214, doi:10.5194/tc-9-2201-2015, 2015.
563 Paul, F.: Repeat Glacier Collapses and Surges in the Amney Machen Mountain Range, Tibet, Possibly Triggered by a
564 Developing Rock-Slope Instability, Remote Sens., 11, 708, doi:10.3390/rs11060708, 2019.

https://doi.org/10.5194/essd-2022-238
Preprint. Discussion started: 11 August 2022

565 Pfeffer, W. T., Arendt, A. A., Bliss, A., Bolch, T., Cogley, J. G., Gardner, A. S., Hagen, J.-O., Hock, R., Kaser, G., Kienholz,
566 C., Miles, E. S., Moholdt, G., Mölg, N., Paul, F., Radić, V., Rastner, P., Raup, B. H., Rich, J., Sharp, M. J., and The Randolph
567 Consortium: The Randolph Glacier Inventory: a globally complete inventory of glaciers, J. Glaciol., 60, 537–552,
568 doi:10.3189/2014JoG13J176, 2014.
569 Purinton, B. and Bookhagen, B.: Beyond Vertical Point Accuracy: Assessing Inter-pixel Consistency in 30 m Global DEMs
570 for the Arid Central Andes, Front. Earth Sci., 9, 758606, doi:10.3389/feart.2021.758606, 2021.
571 Quincey, D. J., Braun, M., Glasser, N. F., Bishop, M. P., Hewitt, K., and Luckman, A.: Karakoram glacier surge dynamics,
572 Geophys. Res. Lett., 38, n/a-n/a, doi:10.1029/2011GL049004, 2011.
573 Rankl, M., Kienholz, C., and Braun, M.: Glacier changes in the Karakoram region mapped by multimission satellite imagery,
574 The Cryosphere, 8, 977–989, doi:10.5194/tc-8-977-2014, 2014.
575 RGI Consortium: Randolph Glacier Inventory - A Dataset of Global Glacier Outlines, Version 6, doi:10.7265/4M1F-GD79,
576 2017.
577 Round, V., Leinss, S., Huss, M., Haemmig, C., and Hajnsek, I.: Surge dynamics and lake outbursts of Kyagar Glacier,
578 Karakoram, The Cryosphere, 11, 723–739, doi:10.5194/tc-11-723-2017, 2017.
579 Sevestre, H. and Benn, D. I.: Climatic and geometric controls on the global distribution of surge-type glaciers: implications
580 for a unifying model of surging, J. Glaciol., 61, 646–662, doi:10.3189/2015JoG14J136, 2015.
581 Shean, D., Shashank Bhushan, Lilien, D., and Meyer, J.: dshean/demcoreg: Zenodo DOI release, Zenodo,
582 doi:10.5281/ZENODO.3243481, 2019.
583 Shean, D. E., Alexandrov, O., Moratto, Z. M., Smith, B. E., Joughin, I. R., Porter, C., and Morin, P.: An automated, open-
584 source pipeline for mass production of digital elevation models (DEMs) from very-high-resolution commercial stereo satellite
585 imagery, ISPRS J. Photogramm. Remote Sens., 116, 101–117, doi:10.1016/j.isprsjprs.2016.03.012, 2016.
586 Shean, D. E., Bhushan, S., Montesano, P., Rounce, D. R., Arendt, A., and Osmanoglu, B.: A Systematic, Regional Assessment
587 of High Mountain Asia Glacier Mass Balance, Front. Earth Sci., 7, 363, doi:10.3389/feart.2019.00363, 2020.
588 Shugar, D. H., Jacquemart, M., Shean, D., Bhushan, S., Upadhyay, K., Sattar, A., Schwanghart, W., McBride, S., de Vries, M.
589 V. W., Mergili, M., Emmer, A., Deschamps-Berger, C., McDonnell, M., Bhambri, R., Allen, S., Berthier, E., Carrivick, J. L.,
590 Clague, J. J., Dokukin, M., Dunning, S. A., Frey, H., Gascoin, S., Haritashya, U. K., Huggel, C., Kääb, A., Kargel, J. S.,
591 Kavanaugh, J. L., Lacroix, P., Petley, D., Rupper, S., Azam, M. F., Cook, S. J., Dimri, A. P., Eriksson, M., Farinotti, D., Fiddes,
592 J., Gnyawali, K. R., Harrison, S., Jha, M., Koppes, M., Kumar, A., Leinss, S., Majeed, U., Mal, S., Muhuri, A., Noetzli, J.,
593 Paul, F., Rashid, I., Sain, K., Steiner, J., Ugalde, F., Watson, C. S., and Westoby, M. J.: A massive rock and ice avalanche
594 caused the 2021 disaster at Chamoli, Indian Himalaya, Science, 373, 300–306, doi:10.1126/science.abh4455, 2021.
595 Steiner, J. F., Kraaijenbrink, P. D. A., Jiduc, S. G., and Immerzeel, W. W.: Brief communication: The Khurdopin glacier surge
596 revisited – extreme flow velocities and formation of a dammed lake in 2017, The Cryosphere, 12, 95–101, doi:10.5194/tc-12-
597 95-2018, 2018.
598 Surazakov, A. and Aizen, V.: Positional Accuracy Evaluation of Declassified Hexagon KH-9 Mapping Camera Imagery,
599 Photogramm. Eng. Remote Sens., 76, 603–608, doi:10.14358/PERS.76.5.603, 2010.
600 Vale, A. B., Arnold, N. S., Rees, W. G., and Lea, J. M.: Remote Detection of Surge-Related Glacier Terminus Change across
601 High Mountain Asia, Remote Sens., 13, 1309, doi:10.3390/rs13071309, 2021.
602 Vijay, S. and Braun, M.: Early 21st century spatially detailed elevation changes of Jammu and Kashmir glaciers (Karakoram–
603 Himalaya), Glob. Planet. Change, 165, 137–146, doi:10.1016/j.gloplacha.2018.03.014, 2018.
604 Yamazaki, D., Ikeshima, D., Tawatari, R., Yamaguchi, T., O'Loughlin, F., Neal, J. C., Sampson, C. C., Kanae, S., and Bates,
605 P. D.: A high-accuracy map of global terrain elevations, Geophys. Res. Lett., 44, 5844–5853, doi:10.1002/2017GL072874,
606 2017.

https://doi.org/10.5194/essd-2022-238
Preprint. Discussion started: 11 August 2022

607 Yasuda, T. and Furuya, M.: Dynamics of surge-type glaciers in West Kunlun Shan, Northwestern Tibet: SURGE-TYPE
608 GLACIERS IN WEST KUNLUN SHAN, J. Geophys. Res. Earth Surf., 120, 2393–2405, doi:10.1002/2015JF003511, 2015.
609 Zhou, S., Yao, X., Zhang, D., Zhang, Y., Liu, S., and Min, Y.: Remote Sensing Monitoring of Advancing and Surging Glaciers
610 in the Tien Shan, 1990–2019, Remote Sens., 13, 1973, doi:10.3390/rs13101973, 2021.
611 Zhou, Y., Li, Z., and Li, J.: Slight glacier mass loss in the Karakoram region during the 1970s to 2000 revealed by KH-9
612 images and SRTM DEM, J. Glaciol., 63, 331–342, doi:10.1017/jog.2016.142, 2017.

613 Tables and Figures

614 **Tabel 1: Surge-type glacier identification results**

Periods	Identified surge-type glaciers									
	Multiple		Verified		Probable		Possible		Total	
	Number	Area (km^2)	Number	Area (km^2)	Number	Area (km^2)	Number	Area (km^2)	Number	Area (km^2)
2000-2010s	52	7919.94	491	7598.72	170	2918.80	94	875.08	807	19312.53
1970s-2000	35	6312.48	343	7920.18	122	1893.47	70	1374.89	570	17501.04
1970s-2010s	70	9112.97	634	9953.32	196	2450.24	115	1249.99	1015	22766.52

615 * The identified surge-type glaciers in 2000-2010s and 1970s-2000partly coincide with each other.
616

617 **Tabel 2: Results of surge-type glacier identification in 22 subregions of HMA. Only glaciers larger than 0.3 km^2 were considered in**
618 **the glacier number related values.**

Regions	Glacier number			Glacier area (km^2)		
	Total	Surge-type	Ratio (%)	Total	Surge-type	Ratio (%)
Karakoram	4754	374	7.87	21475.07	11324.78	52.73
Western Pamir	3612	200	5.54	7836.76	3030.59	38.67
Western Kunlun Shan	2844	96	3.38	8456.79	2936.28	34.72
Eastern Pamir	1154	67	5.81	2699.30	968.44	35.88
Central Tien Shan	2591	62	2.39	7270.02	1414.46	19.46
Tibetan Interior Mountains	1538	33	2.15	3815.20	553.89	14.52
Central Himalaya	3686	29	0.79	8681.43	303.08	3.49
Northern and Western Tien Shan	1596	26	1.63	2261.39	164.67	7.28
Eastern Kunlun Shan	1368	23	1.68	2994.99	593.78	19.83
Tanggula Shan	760	19	2.50	1840.75	391.22	21.25
Eastern Hindu Kush	1610	16	0.99	2938.45	265.51	9.04
Nyainqentanglha	3315	16	0.48	7046.71	226.91	3.22
Pamir Alay	1195	15	1.26	1846.03	188.63	10.22
Western Himalaya	4279	14	0.33	7986.95	182.53	2.29
Qilian Shan	1032	7	0.68	1597.68	62.16	3.89
Eastern Himalaya	1351	5	0.37	2844.34	83.12	2.92
Eastern Tibetan Mountains	176	4	2.27	312.13	36.99	11.85
Altun Shan	177	4	2.26	295.14	6.67	2.26
Eastern Tien Shan	1463	3	0.21	2333.16	13.41	0.57
Gangdise Mountains	968	1	0.10	1270.72	11.18	0.88
Hengduan Shan	862	1	0.12	1281.93	8.22	0.64
Dzhungarsky Alatau	400	0	0	520.89	0	0
Total	40731	1015	2.49	97605.85	22766.52	23.32

https://doi.org/10.5194/essd-2022-238
Preprint. Discussion started: 11 August 2022

619 **Table 3: Attribute information in the present surge-type glacier inventory.**

Attribute	Description	Attribute	Description
RGIId	RGI identifier	Aspect	Mean glacier aspect/orientation (°)
GLIMSId	GLIMS identifier	Slope	Mean glacier mean surface slope (°)
CenLon	Longitude of the glacier centroid (°)	Lmax	Maximum length of glacier flow line (m)
CenLat	Latitude of the glacier centroid (°)	Name	Name of the glacier
Area	Glacier covered area (km^2)	Surge(10s)	Surge occurred during 2000-2010s
Zmin	Minimum elevation of the glacier (m a.s.l)	Surge(70s)	Surge occurred during 1970s-2000
Zmax	Maximum elevation of the glacier (m a.s.l)	Surgetype	Final surge identification during 1970s-2010s
Zmed	Median elevation of the glacier (m a.s.l)	HiMAP_region	HMA subregion that the glacier belongs to

620

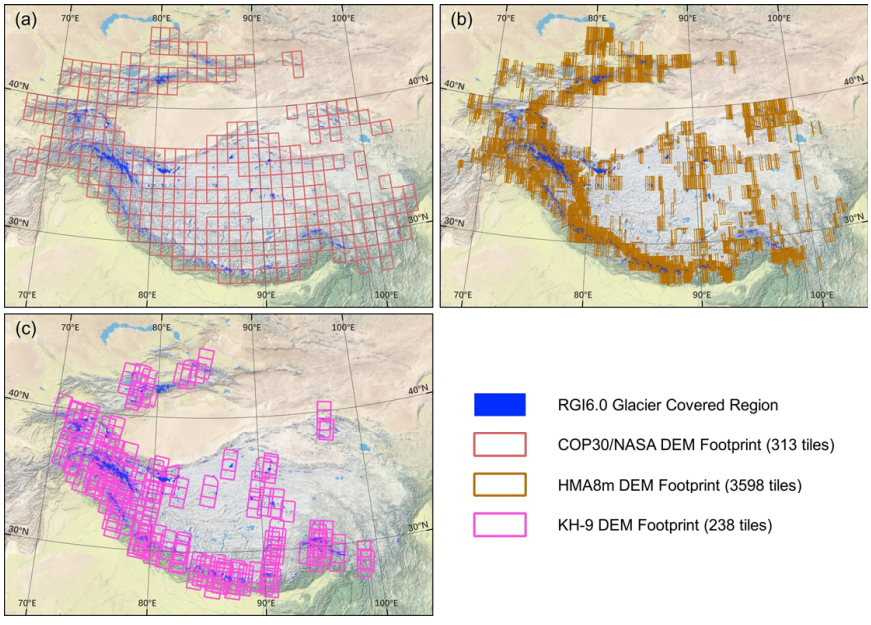

621

622 **Figure 1: Footprints of (a) COP30/NASA DEMs, (b) HMA8m DEMs, and (c) KH-9 DEMs that were utilized in this study. The**
623 **background is rendered from the ESRI World Physical base map (Source: US National Park Service).**

https://doi.org/10.5194/essd-2022-238
Preprint. Discussion started: 11 August 2022

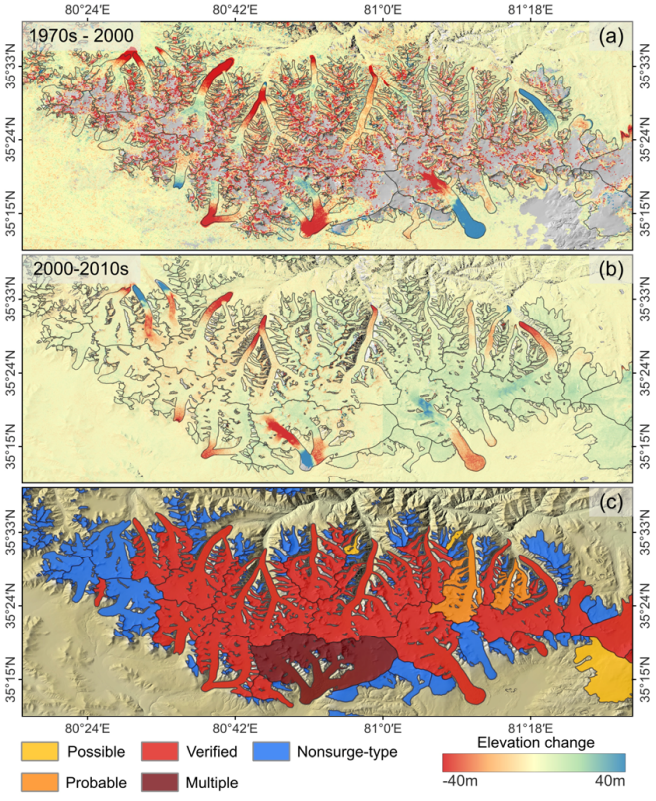

Figure 2: An example of derived elevation change maps during 1970s-2000 (a) and 2000-2010s (b), and the corresponding surge-type glacier identification result (c). Black curves are glacier outlines. The background is the shaded relief of COP30 DEM (Source: ESA). The area is located in the main massif of Western Kunlun Shan.

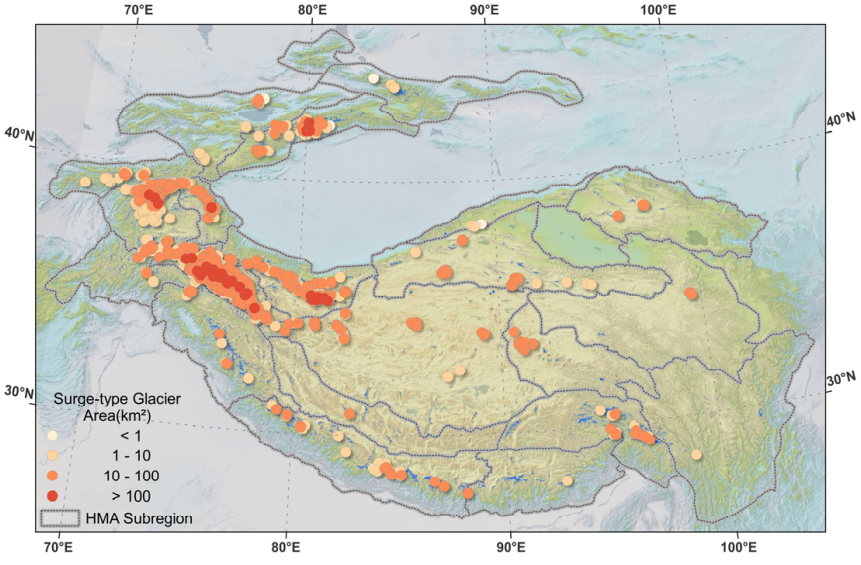

Figure 3: Overview of the distribution of identified surge-type glaciers in 22 subregions of HMA. The background is the shaded relief of SRTM DEM (Source: USGS).

https://doi.org/10.5194/essd-2022-238
Preprint. Discussion started: 11 August 2022

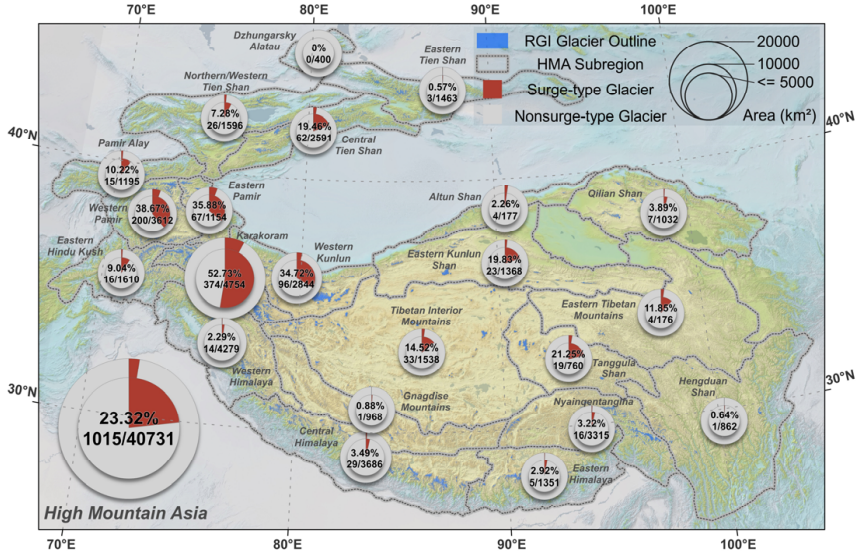

631

632 **Figure 4: Distribution of surge-type glaciers in the 22 subregions of HMA. The double-level pie chart represents the ratios of surge-**
633 **type glacier number and area in each subregion. The inner pie denotes the area ratio labelled by a percentage, and the outer pie**
634 **denotes the number ratio labelled by a fraction (only considered glacier larger than 0.3 km^2). The background is the shaded relief**
635 **of SRTM DEM (Source: USGS).**

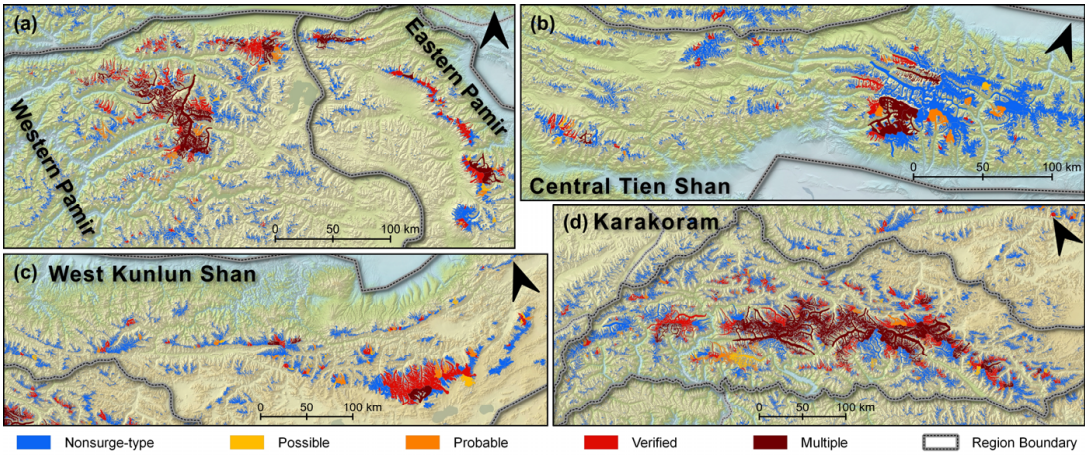

636

637 **Figure 5: Results of surge-type glacier identification in the Pamirs (a), Central Tien Shan (b), West Kunlun Shan (c), and Karakoram**
638 **(d). The background is the shaded relief of SRTM DEM (Source: USGS).**

https://doi.org/10.5194/essd-2022-238
Preprint. Discussion started: 11 August 2022

Open Access Earth System Science Data Discussions

Area Class (km^2)	Total		Surge-type		Ratio	
	Count	Area	Count	Area	Count	Area
0.3-0.5	12192	4748.8	5	2.2	0.04	0.05
0.5-1	12549	8842.6	20	16.2	0.16	0.18
1-3	10716	17946.7	176	344.7	1.64	1.92
3-5	2343	8981.6	143	567.1	6.10	6.31
5-10	1672	11495.0	247	1807.8	14.77	15.73
10-30	939	15273.8	274	4656.6	29.18	30.49
30-50	150	5739.1	67	2591.3	44.67	45.15
50-100	85	6073.2	48	3480.9	56.47	57.31
100-300	36	5771.5	25	3856.2	69.44	66.82
300-500	7	2706.8	6	2332.9	85.71	86.19
>500	4	3110.6	4	3110.6	100.00	100.00

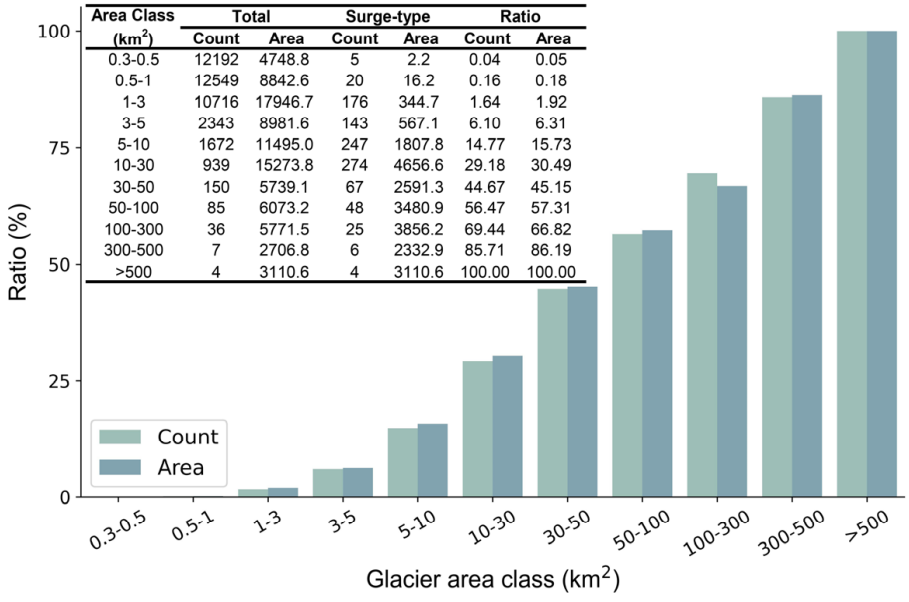

Figure 6: The ratios of surge-type glacier number and area in different classes.

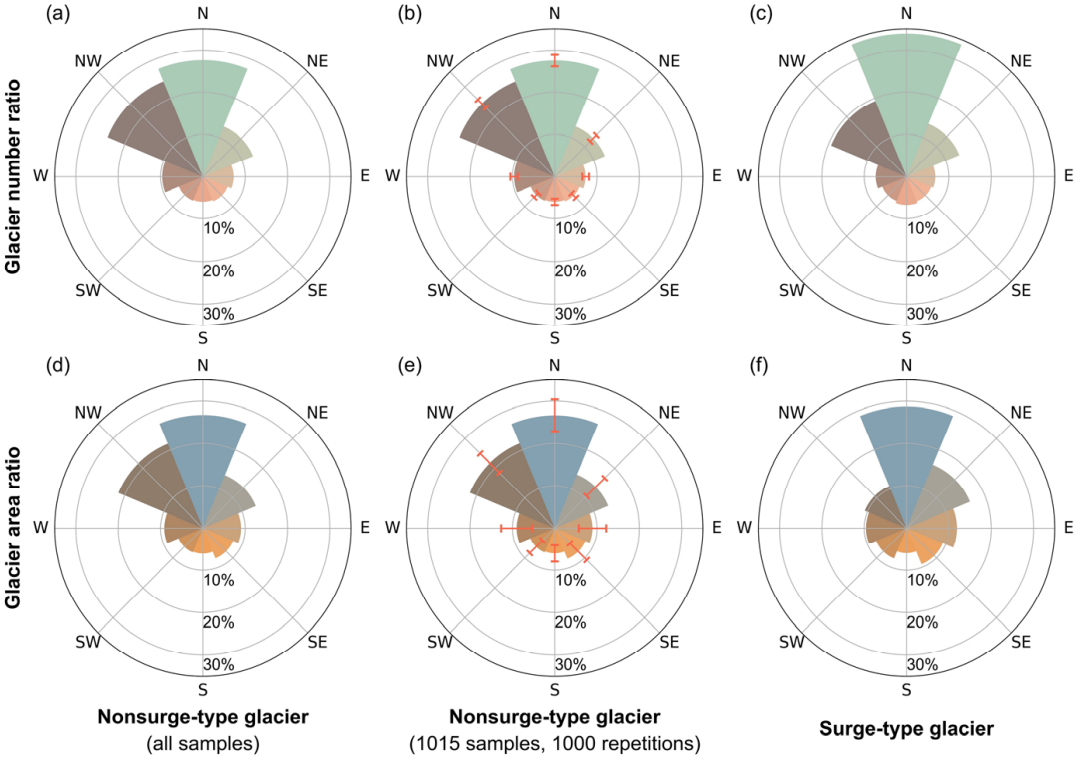

Figure 7: The distribution of glacier number and area in eight aspects. The upper row: glacier number ratio; lower row: glacier area ratio. Left column: distribution of all nonsurge-type glaciers; center column: averaged distribution of 1015 random nonsurge-type glacier samples with 1000 repetitions, the error bar denotes the STD calculated from the 1000 repetitions of nonsurge-type glacier samples ; right column: distribution of surge-type glacier. Glaciers smaller than 0.3 km^2 were excluded in the nonsurge-type glaciers class.

https://doi.org/10.5194/essd-2022-238
Preprint. Discussion started: 11 August 2022

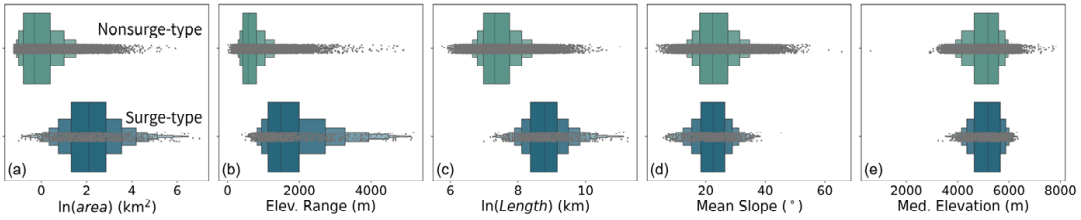

Figure 8: The comparison between the boxplots of geometric properties of nonsurge-type and surge-type glaciers. (a) Natural logarithm of area. (b) elevation range. (c) Natural logarithm of length. (d) Mean surface slope. (e) Median elevation. Glaciers smaller than 0.3 km² were excluded in the nonsurge-type glaciers class.

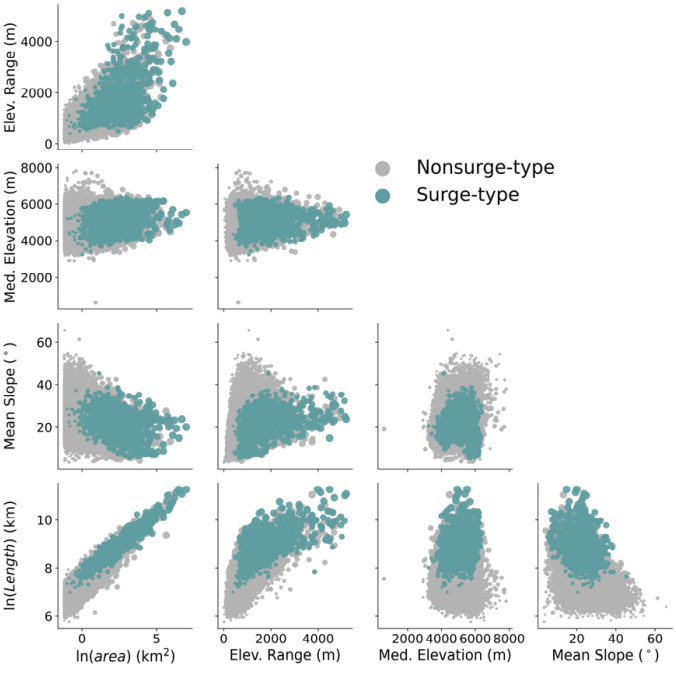

Figure 9: Bivariate scatterplots of geometric properties of nonsurge-type and surge-type glaciers. The larger dots represent larger glaciers. Glaciers smaller than 0.3 km² were excluded in the nonsurge-type glaciers class.

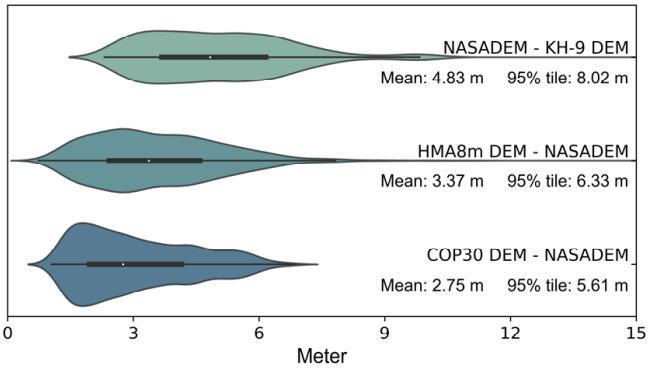

Figure 10: The distribution of NMAD of elevation change observations in stable areas of all DEM differencing tiles. In each category, the shaded area denotes the density distribution of the NMAD of all DEM differencing tiles. The white dot denotes the median in each group. The thick line represents the interquartile range (IQR, i.e., 75th percentile-25th percentile) in each group. The thin line represents the range between the minimum value (25th percentile - 1.5IQR) and the maximum value (75th percentile + 1.5IQR).